Aptamer-assisted tumor localization of bacteria for enhanced biotherapy

Zhongmin Geng
Shanghai Jiao Tong University
Zhenping Cao
Shanghai Jiao Tong University
Rui Liu
Shanghai Jiao Tong University
Ke Liu
Shanghai Jiao Tong University
Jinyao Liu (jyliu@sjtu.edu.cn)
Shanghai Jiao Tong University https://orcid.org/0000-0002-6044-2033
Weihong Tan
Hunan University https://orcid.org/0000-0002-8066-1524

Article

Keywords: Bacteria, Aptamer, Conjugate, Biotherapy, Tumor

Posted Date: July 12th, 2021

DOI: https://doi.org/10.21203/rs.3.rs-663226/v1

Version of Record: A version of this preprint was published at Nature Communications on November 15th, 2021. See the published version at https://doi.org/10.1038/s41467-021-26956-8.

Aptamer-assisted tumor localization of bacteria for enhanced biotherapy

Zhongmin Geng[1], Zhenping Cao[1], Rui Liu[1], Ke Liu[1], Jinyao Liu[1,2]*, Weihong Tan[1]*

[1]Shanghai Key Laboratory for Nucleic Acid Chemistry and Nanomedicine, Institute of Molecular Medicine, State Key Laboratory of Oncogenes and Related Genes, Renji Hospital, School of Medicine, Shanghai Jiao Tong University, Shanghai 200127, China.

[2]Shanghai Key Laboratory of Gynecologic Oncology, Renji Hospital, School of Medicine, Shanghai Jiao Tong University, Shanghai 200127, China.

*Corresponding authors E-mail: jyliu@sjtu.edu.cn; tan@hnu.edu.cn

ABSTRACT

Despite bacterial-mediated biotherapies have been widely explored for treating different types of cancer, their implementation has been restricted by severe side effects and low treatment efficacies, due largely to the absence of tumor-specific accumulation following administration. Here, the conjugation of aptamers to bacterial surface is described by a simple and cytocompatible amidation procedure, which can significantly promote the localization of bacteria in tumor site after systemic administration. The surface density of aptamers can be easily adjusted by varying feed ratio and the conjugation is able to increase the stability of anchored aptamers. Optimal bacteria conjugated with an average of 2.8×10^5 aptamers per cell present the highest specificity to tumor cells in vitro, separately generating near 2- and 5-times higher accumulation in tumor tissue at 12 and 60 hours compared to unmodified bacteria. In both 4T1 and H22 tumor-bearing mouse models, aptamer-conjugated attenuated Salmonella show strikingly enhanced antitumor efficacy, along with highly activated immune responses inside the tumor. This work demonstrates how bacterial behaviors can be tuned by surface conjugation and supports the potential of aptamer-conjugated bacteria for both targeted intratumoral localization and enhanced tumor biotherapy.

KEYWORDS

Bacteria; Aptamer; Conjugate; Biotherapy; Tumor

INTRODUCTION

In the late 19th century, W. Busch and W. Coley have independently utilized *Streptococcus pyrogens* and *Serratia marcescens* to treat cancer, which appears distinct tumor suppression effects in some sarcoma patients.[1, 2] Since then, the exploration of bacterial-based tumor therapies never stops, although the therapeutic outcomes of these treatments remain unstable.[3] Particularly, with recent progress in the fields of immunology and biotechnology, bacteria have attracted increasing attention in tumor biotherapy, both as immune modulators and drug delivery vehicles.[4, 5] The infection by bacteria is able to promote the immunogenicity of tumors, which further induces effective antitumor immune responses.[6] As reported, different immune cell subtypes, such as $CD4^+$ and $CD8^+$ T cells, regulatory T cells, and tumor-associated macrophages, can be modulated to generate antitumor immunity by attenuated bacteria.[7] Furthermore, the colonization of bacteria in tumor tissue is capable to trigger the activation of innate immunocytes and the release of proinflammatory factors, which cause the disruption of tumor vasculature as well as the associated thrombosis.[8] Regarding the application of bacteria as drug carriers, the greatest strength is their favorable colonization in tumor site, which is attributed to the intratumor anaerobic condition, eutrophication, and the immunosuppressive microenvironment.[9-11] Namely, the use of bacteria as delivery vehicles can improve the accumulation and penetration of drugs in tumor tissue and hence maximize their therapeutic efficacies. Unfortunately, bacterial-mediated tumor therapy always suffers from low inhibition efficiency of tumor growth and undesirable dose-dependent side

effects, as confirmed in the failure of phase 1 clinical trial of attenuated *Salmonella typhimurium*.[12]

Substantial efforts have been made to tackle these challenges by modifying bacteria either chemically or genetically.[13, 14] To reduce systemic toxicity, several bacterial species including *Listeria*, *Escherichia coli*, and *Clostridium* have been attenuated by removing key virulence factor genes.[15] Alternatively, decoration with various types of substrates on bacterial surface, such as synthetic nanoparticles and therapeutic drugs, has been exploited to enhance antitumor activity.[16-19] We have recently wrapped with extra coatings to retain bacterial viability under unfriendly external conditions.[20-24] For instance, bacteria decorated with a stealth coating can decrease their elimination by macrophages, which subsequently prolongs blood circulation following systemic injection.[25] However, previous modifications by both chemical and genetical approaches lack the ability to endow bacteria with increment in tumor-specific localization after administration. Therefore, new strategies are highly desirable for increasing the tumor-targeting capacity of bacteria, which can in turn increase the safety and antitumor efficacy of bacterial-based therapy.

Aptamers, which are considered as “chemical antibodies”, have been broadly applied as targeting ligands due to their ability to specifically recognize cell-surface targets (such as nucleic acids and proteins), whole cells, and even tissues.[26-28] Similar to antibodies, aptamers exhibit many favorable features including high affinity, excellent specificity, and low immunogenicity.[29] In addition, aptamers can be easily

synthesized in vitro through mature solid state synthetic technology and be chemically modified with various functional groups.[30] By virtue of these unique characteristics, several therapeutic aptamers have been evaluated in clinical trials for their potential in cancer treatment.[31] However, aptamer-based drug delivery has been mainly focused on developing aptamer-drug conjugates and aptamer-functionalized nanoparticles, with aims to enhance antitumor efficacies by increasing the accumulation of drugs in tumors.[32-34] To the best of our knowledge, the use of aptamers to actively deliver living cells to tumor site by a specific ligand-receptor interaction has not been reported yet.

In this work, we describe aptamer-assisted tumor localization of bacteria for enhanced biotherapy (**Figure 1**). Tumor-specific aptamers have been conjugated to the surface of bacteria by a single-step amidation procedure, which produces aptamer-conjugated bacteria (ApCB). The preparation shows negligible influence on bacterial viability, as the obtained ApCB grow similarly to unmodified bacteria. The grafting density of aptamers on bacteria surface can be readily tuned from 0.7×10^5 to 5.7×10^5 aptamers per cell by controlling feed ratio. More importantly, the attachment is capable of decreasing the enzymatic hydrolysis of aptamers anchored on the surface, as up to 80% of which remains intact after 24 hours exposure to serum. Among a set of ApCB with different grafting densities, bacteria decorated with an average of 2.8×10^5 aptamers per cell exhibit the highest specificity to tumor cells in vitro, which separately achieves 2- and 5-fold higher colonization in tumor tissue at 12 and 60 hours post tail vein injection in mice. As a proof-of-concept study,

aptamer-conjugated attenuated *Salmonella Typhimurium VNP20009* (VNP) display significantly enhanced antitumor efficacy in both 4T1 and H22 tumor-bearing mouse models, accompanied with remarkably elicited immune responses within the tumor. Therefore, our work illustrates a unique strategy to manipulate bacterial behaviors by simple surface modification and demonstrates the promising of ApCB for enhanced bacterial-mediated cancer therapy.

RESULTS AND DISCUSSION

Preparation and characterization of ApCB

In view of the specificity to bind with nucleolin overexpressing on the membrane of various cancer cells,[35] we selected aptamer AS1411 to prepare ApCB. On the other hand, a well-known probiotic bacterium, *Escherichia coli Nissle* 1917 (EcN), was chosen as a model strain due to its ability to colonize in different tumors.[36] By amide condensation, aminated AS1411 was linked to the carboxyl group of *N*-acetylmuramic acid (**Figure 1**a), which extensively exists in the cell wall of Gram-negative bacteria.[37] With the help of 1-ethyl-3-(3-dimethylaminopropyl)carbodiimide (EDC) and *N*-hydroxysuccinimide (NHS), ApCB were prepared by co-incubating EcN with AS1411 in phosphate buffered saline (PBS) at room temperature for 3 hours and the resulting bacteria were purified simply by centrifugation. To enable the measurement by laser scanning confocal microscopy (LSCM) and flow cytometry, AS1411 labelled with fluorochrome Cyanine5 (Cy5) at 5’ end of the sequence was used to prepare ApCB.

As visualized in **Figure 1**c, LSCM images showed that EcN expressing green fluorescent protein (GFP) were efficiently decorated with AS1411 (red) under the experimental condition. Successful decoration with AS1411 was further confirmed by flow cytometric analysis. The mean fluorescence intensity of ApCB was around 10-times higher than that of EcN (Supplementary **Figure S1**), indicating that bacteria were conjugated with Cy5-labelled AS1411.

Given that the surface density of aptamers could influence the binding ability of the modified bacteria,[38] we then investigated whether the number of grafted aptamers could be tuned by varying feed ratio. A given amount of 1×10^8 colony forming units (CFU) of EcN were incubated with 0, 2, 5, and 10 nmol of AS1411, which were termed as EcN, 2ApCB, 5ApCB, and 10ApCB, respectively. Then, the resulting bacteria were analyzed by flow cytometry. As expected, the fluorescence signals increased with the concentration of AS1411, as revealed clearly by a continuous shift of the curve to a higher intensity (**Figure 1**d and e). These results suggested a concentration-dependent conjugation, which meant that the grafting density of AS1411 could be controlled through changing the feed ratio. To calculate the number of grafted aptamers per cell, EcN conjugated with different concentrations of Cy5-labelled AS1411 were detected by fluorescence spectrophotometer. The number of aptamers decorated on bacteria was quantified by calculating the difference of fluorescent intensity of the aptamer solution after reaction. In good agreement with the result of flow cytometric analysis, the number of attached aptamers increased with the incubation concentration of AS1411, as illustrated in **Figure 1**f. The quantities of

AS1411 conjugated on the surface of 2ApCB, 5ApCB, and 10ApCB were calculated to be 0.7×10^5, 2.8×10^5, and 5.7×10^5 aptamers per cell, respectively.

To investigate whether the preparation procedure and the conjugated aptamers had toxic side effects on bacterial viability, the growth of ApCB was assessed using plate counting. Serial dilutions of EcN, 2ApCB, 5ApCB, and 10ApCB were prepared and then spread onto Luria Bertani (LB) agar plates. After incubation at 37 °C for 24 hours, the viability of ApCB was determined by recording the number of bacterial colonies. As shown in **Figure 1**g, in contrast to EcN, 2ApCB, 5ApCB, and 10ApCB displayed no notable difference in colony number, verifying the uninfluenced bacterial viability after conjugation. In addition, the serum tolerance of an aptamer-based therapeutic agent is critical for in vivo applications.[39] We speculated that the conjugation of aptamers on the surface of bacteria could largely increase the steric hindrance towards the enzymatic hydrolysis of AS1411 by nucleases.[40] To demonstrate this hypothesis, the stability of aptamers decorated on EcN was monitored by tracking the fluorescence intensity of Cy5-labelled AS1411. ApCB were analyzed by flow cytometry after incubation with 90% phosphate-buffered serum at 37 °C for the predetermined time points. On the basis of our previous report, more than 60% of free AS1411 was found to be rapidly degraded after 48 hours incubation.[33] Extraordinarily, the stability of AS1411 grafted to the surface of EcN was greatly improved under the same experimental condition, with more than 70% of the conjugated aptamers remaining intact (**Figure 1**h). These data indicated that the

conjugation could strengthen the resistance of aptamers against serum-mediated degradation, suggesting the potential of ApCB to be utilized in vivo.

Increased binding of ApCB with cancer cells

With the guidance of surface-anchored aptamers, we expected that ApCB could present specific affinity to cancer cells overexpressing the corresponding receptors. To examine the role of attached AS1411 on the invasion of EcN to cancer cells, cellular binding efficiencies of EcN, 2ApCB, 5ApCB, and 10ApCB were assessed by using 4T1 cells, a cell line that overexpresses nucleolin. LSCM imaging showed that the attachment of AS1411 to the cell surface could strengthen the binding of EcN with 4T1 cells (**Figure 2**a). Interestingly, incubation with 5ApCB visualized the highest number of bound EcN on the cell surface. Although there was much more grafted AS1411 on EcN surface, 10ApCB bound less efficiently than 5ApCB. This might be ascribed to the influence of grafting density, such as the accessibility of adjacent aptamers as well as the steric effects of neighboring aptamers on the surface.[41] In accordance with the result of confocal imaging, flow cytometric analysis indicated that the binding efficiency increased with the grafting density of AS1411 increasing from 0.5×10^5 to 2.8×10^5 aptamers per cell, while decreased with further increasing the number to 5.5×10^5 (**Figure 2**b). Under the same culture condition, the percentages of 4T1 cells bound with EcN after incubation with EcN, 2ApCB, 5ApCB, and 10ApCB for 2 hours were about 5%, 15%, 50%, and 30%, respectively (**Figure 2**c). These results demonstrated that decoration with aptamers could promote the

interaction of bacteria with targeting cancer cells via specific ligand-receptor recognition, which depended on the grafting density.

To directly visualize the binding of ApCB with cancer cells, 4T1 cells after co-incubation with EcN and 5ApCB were observed by scanning electron miscopy (SEM), respectively (**Figure 3**a). Representative SEM images showed that more bacteria were attached onto the surface of 4T1 cells after culture with 5ApCB instead of EcN, which was consistent with the results of flow cytometric analysis. To verify the specific binding with cancer cells, EcN and 5ApCB were separately added to the culture medium of 293T cells, a cell line that presents low nucleolin expression.[42, 43] Flow cytometric analysis suggested that there was no significant difference in fluorescence intensity between the binding of 293T cells with EcN and 5ApCB (**Figure 3**b and c). Meanwhile, LSCM images displayed that the binding efficiency of 5ApCB with 293T cells was similar to that of EcN, which exhibited limited bacteria attaching onto the surface of 293T cells (**Figure 3**d). These results indicated that the attachment of AS1411 onto bacteria played a critical role for ApCB to specifically bind with cancer cells. Moreover, to further assess the binding efficiency of ApCB with cancer cells in vivo, a 4T1 tumor model was developed and the obtained tumor-bearing mice were intravenously dosed with PBS and 1×10^7 CFU of VNP or 5ApCB, respectively. Tumor tissues were sampled and stained with both FITC-labelled anti-*Escherichia coli* and 4',6-diamidino-2-phenylindole (DAPI) at 12 hours post-injection (**Figure 3**e). Clearly, mice injected with 5ApCB presented a largely increased number of bacteria binding with cancer cells compared to EcN,

further demonstrating the specific and enhanced binding of bacteria by conjugation with aptamers on the surface.

Having confirmed the presence of exogenous function that could specifically bind with tumor cells after conjugation, we next turned our attention to evaluate the ability of ApCB to target tumor site. The tumor targeted colonization of ApCB was determined by tumor imaging using a 4T1 tumor-bearing mouse model. Based on the result of in vitro assay, 5ApCB with the highest binding efficiency were used to evaluate the tumor accumulation. To enable visual tracking, luxCDABE engineered 5ApCB were intravenously injected into the tumor-bearing mice through tail vein, while engineered EcN without surface aptamers were administered as a control. At the indicated time points post-injection, the dosed mice were observed by in vivo imaging system (IVIS). As shown in **Figure 4**a and b, the average luminescence signals in the tumors obtained by IVIS increased continuously with the time interval increasing from 12 to 60 hours post-administration. Importantly, at each time point, the average intensity of luminescence signals from the tumor site in mice injected with 5ApCB was significantly higher than that of mice treated with unconjugated bacteria. Particularly, at 60 hours after injection, the relative signal intensity was 5-fold higher than that of the control group. To quantify the tumor colonization, the biodistribution of the bacteria was examined at the end point of the animal study. After euthanasia, the heart, kidney, liver, lung, spleen, and tumor tissues were collected and then homogenized before spreading onto LB agar plates for bacterial counting. Accordantly, the bacterial number in the tumor tissue sectioned from mice injected

with 5ApCB reached to 5-times higher than that of the control mice (**Figure 4**c). In contrast to the major organs, the distribution of bacteria in the tumor tissue was extraordinary, with around 99.9% of total bacteria colonizing inside the tumor. The overwhelming aggregation of EcN within the tumor tissue was ascribed to their preference for hypoxic, eutrophication, and the immunosuppressive microenvironment of tumors.[44] Speculatively, in comparison to undecorated EcN, the notably enhanced accumulation within the tumor tissue after injection with 5ApCB was attributed to the improved localization of bacteria following administration, which was resulted from the specific binding with tumor cells. To prove this assumption, the localization of EcN within the 4T1 tumor at a relative short period of time after injection was quantified by plate counting. As confirmed in **Figure 4**d and Supplementary **Figure S2**, the number of bacteria localized into the tumor at 12 hours after dosing with 5ApCB achieved 1.75×10^7 CFU per gram tissue, which was 2-fold higher than that of unconjugated EcN. Namely, surface conjugation indeed offered a greater opportunity to localize tumor site through a ligand-receptor interaction between aptamer-decorated bacteria and the tumor cells.

Enhanced anticancer efficacy of ApCB

To validate the versatility of our approach, we translated the surface conjugation of aptamers to VNP, a well-known strain that has been widely used for tumor biotherapy due to its high immunogenicity.[45] VNP were similarly conjugated with AS1411 (Supplementary **Figure S3**) and the antitumor efficacy of the resulting 5ApCB was

assessed in vivo. Mouse subcutaneous tumor model of 4T1 was employed and the obtained tumor-bearing mice were randomly divided into three groups (n = 5) that were received with different treatments including PBS, VNP and 5ApCB. Each mouse in VNP and 5ApCB groups was intravenously injected with 5×10^5 CFU of bacteria at day 0. A tumor inhibition study by concisely assessing tumor volume demonstrated that both VNP and 5ApCB could inhibit tumor growth compared to PBS group (**Figure 5**a and b). Expectedly, 5ApCB group showed significantly enhanced antitumor efficacy in comparison with VNP group, suggesting that the increased tumor localization enabled by surface conjugation of aptamers played an important role in tumor biotherapy. Furthermore, the variation of bodyweight recorded every other day after treatment revealed the limited side effects of the bacteria under the experimental dosage. As displayed in **Figure 5**c, although the bodyweight of mice dropped slightly after injection with the bacteria, the mice in both VNP and 5ApCB groups recovered rapidly as reflected by the return of the bodyweight to the same level of PBS group.

It has been reported that the colonization of *Salmonella* can provoke the immunosuppressive microenvironment of tumors and elicit antitumor immunity.[46] To disclose the bacterial-mediated immune responses, the activation of T cells in the tumor tissue was analyzed at the end of the treatment. Nuclear nonhistone protein Ki67 was used as a maker to detect the infiltration of $CD3^+$ T cells in the tumor.[47] As shown in **Figure 5**d and Supplementary **Figure S4**a, the proliferation of $CD3^+$ T cells in mice treated with 5ApCB presented an apparent increase in contrast to both

PBS and VNP groups. Moreover, treatment with 5ApCB significantly elevated the percentage of $CD3^+CD4^+$ T cells (**Figure 5**e and Supplementary **Figure S4**b), which suggested that the aptamer-decorated bacteria could boost more efficient tumor infiltration of immunologic effector cells. The percentage of tumor cytokine interferon-γ (IFN-γ) and tumor necrosis factor-α (TNF-α), which predominantly regulates the cell-mediated immune responses,[48] was further examined and the results showed a striking increase in mice treated with 5ApCB (**Figure 5**f and g, Supplementary **Figure S4**c and **S5**a). Terminal deoxynucleotidyl transferase dUTP nick end labeling (TUNEL) staining depicted the highest level of tumor cell apoptosis induced by 5ApCB (**Figure 5**h and Supplementary **Figure S5**b). In addition, hematoxylin and eosin (H&E) staining exhibited prominent necrosis of the tumor tissues after treatment with the conjugated bacteria (**Figure 5**i). Taken together, the inhibition of tumor growth could be attributed to the aptamer-mediated enhanced localization in tumor site and the bacterial associated activation of antitumor immune responses.

Versatility of ApCB

To explore the generality of this strategy as a versatile platform for different aptamers, TLS11a was selected and the corresponding tumor model of H22 hepatocellular carcinoma was used to evaluate the effectiveness of conjugating aptamers to bacterial surface.[49, 50] TLS11a based ApCB (T-ApCB) was synthesized similarly by co-incubating amino-functionalized TLS11a with VNP (**Figure 6**a). Details for the

preparation of T-ApCB were described in the Supplementary Information. Correspondingly, T-5ApCB were fabricated by incubation of 1×10^8 CFU of VNP with 5 nmol of TLS11a. Flow cytometric analysis showed that H22 cells co-incubated with T-5ApCB presented stronger fluorescence intensity than those cultivated with VNP, demonstrating strengthened affinity of conjugated bacteria to bind with cancer cells (**Figure 6**b). We next evaluated the antitumor efficacy of the resulting T-5ApCB in H22 tumor-bearing mice. After a single intravenous injection of PBS, 5×10^5 CFU of VNP or T-5ApCB at day 0 (tumor size ~100 mm^3), both the tumor size and body weight of the treated mice were recorded. As plotted in **Figure 6**c and d, T-5ApCB group appeared a significant inhibition of tumor growth in comparison with PBS and VNP groups, which could be explained by that surface conjugation of aptamers increased the intratumoral localization of bacteria. Survival rate of different groups further validated that treatment with T-5ApCB endowed H22 tumor-bearing mice with a significantly extended survival period, as reflected by that near 70% of the treated mice survived successfully in 36 days (**Figure 6**e). While, none of mice dosed with PBS or VNP could survive under the same conditions. In addition, the variation of body weight during treatment revealed that administration with bacteria slightly dropped mouse body weight, which recovered rapidly to the same level of PBS group (**Figure 6**f). The slight fluctuation in body weight implied the limited side effects of 5ApCB at the experimental dosage. Collectively, these results proposed the universality of this approach to prepare diverse ApCB and verified the ability of

ApCB to increase the localization of conjugated bacteria in solid tumors for enhanced biotherapy.

CONCLUSION

In summary, we have reported a strategy of conjugating aptamers to bacterial surface for endowing bacteria with tumor-specific accumulation following administration. The conjugation is based on a single-step and cytocompatible amidation procedure, which is implementable to diverse Gram-negative bacteria. The grafting density of aptamers on bacterial surface can be simply controlled by tuning feed ratio and the attachment is capable to increase the resistance of anchored aptamers against degradation due to the increase of steric hindrance towards the enzymatic hydrolysis by nucleases. With an optimized number of 2.8×10^5 aptamers per cell, the conjugated bacteria exhibit the highest specific affinity with tumor cells in vitro. Strikingly, the optimal bacteria reached near 2- and 5-fold higher colonization in tumor tissue at 12 and 60 hours after systemic administration in vivo. The therapeutic value in tumor biotherapy has been validated by injection with aptamer-conjugated attenuated *Salmonella* in both 4T1 and H22 tumor-bearing mice. As expected, the decorated bacteria display significantly enhanced antitumor efficacy, with effective infiltration of immunologic effector cells and expression of tumor cytokines inside the tumor. This work discloses how bacterial bioactivities can be manipulated by surface conjugation with aptamers. With potential to address the severe side effects and low efficacy associated with bacterial-based therapy, we anticipate the application of this

strategy as a versatile platform to develop various bacterial therapeutics for enhanced tumor treatment.

SUPPLEMENTARY DATA

Supplementary data are available.

FUNDING

This work is supported by the National Natural Science Foundation of China (21875135), the Recruitment Program of Global Youth Experts of China (D1410022), the Shanghai Municipal Education Commission-Gaofeng Clinical Medicine Grant Support (20181704, 20191820), and the Innovative Research Team of High-Level Local Universities in Shanghai (SSMU-ZLCX20180701).

AUTHOR CONTRIBUTIONS

J.L. and W.T. supervised the project. J.L. conceived and designed the experiments with Z.G. Z.G., Z.C., R.L. and K.L. performed all experiments. All authors analysed and discussed the data. Z.G. and J.L. wrote the paper.

Conflict of interest

The authors declare no conflict of interest.

REFERENCES

1. Busch, W. Aus der Stizung der medizinischen section vom 13. November 1867. *Berl Klin Wochenschr* 1868; **5**(5): 137.

2. Coley, WB. The treatment of malignant tumors by repeated inoculations of erysipelas. With a report of ten original cases. 1893. *Clin Orthop Relat Res*. 1991; **262:** 3-11.

3. Huo, M, Wang, L, Zhang, L*, et al.* Photosynthetic Tumor Oxygenation by Photosensitizer-Containing Cyanobacteria for Enhanced Photodynamic Therapy. *Angew Chem Int Ed*. 2020; **59**(5): 1906-13.

4. Romero, D. Oncolytic viruses prime antitumour immunity. *Nat Rev Clin Oncol*. 2018; **15**(3): 135.

5. Duong, MT-Q, Qin, Y, You, S-H*, et al.* Bacteria-cancer interactions: bacteria-based cancer therapy. *Exp Mol Med*. 2019; **51**(12): 1-15.

6. Hu, Q, Wu, M, Fang, C*, et al.* Engineering Nanoparticle-Coated Bacteria as Oral DNA Vaccines for Cancer Immunotherapy. *Nano Lett*. 2015; **15**(4): 2732-9.

7. Chen, Q, Bai, H, Wu, W*, et al.* Bioengineering Bacterial Vesicle-Coated Polymeric Nanomedicine for Enhanced Cancer Immunotherapy and Metastasis Prevention. *Nano Lett*. 2020; **20**(1): 11-21.

8. Yi, X, Zhou, H, Chao, Y*, et al.* Bacteria-triggered tumor-specific thrombosis to enable potent photothermal immunotherapy of cancer. *Sci Adv*. 2020; **6**(33): eaba3546.

9. Chen, Q-W, Liu, X-H, Fan, J-X*, et al.* Self-Mineralized Photothermal Bacteria Hybridizing with Mitochondria-Targeted Metal–Organic Frameworks for Augmenting Photothermal Tumor Therapy. *Adv Funct Mater*. 2020; **30**(14): 1909806.

10. Zheng, DW, Chen, Y, Li, ZH*, et al.* Optically-controlled bacterial metabolite for cancer therapy. *Nat Commun*. 2018; **9**(1): 1680.

11. Zhou, S, Gravekamp, C, Bermudes, D*, et al.* Tumour-targeting bacteria engineered to fight cancer. *Nat Rev Cancer*. 2018; **18**(12): 727-43.

12. Lee, CH, Wu, CL, Chen, SH*, et al.* Humoral immune responses inhibit the antitumor activities mediated by Salmonella enterica serovar choleraesuis. *J Immunother*. 2009; **32**(4): 376-88.

13. Stauber, RH, Siemer, S, Becker, S*, et al.* Small Meets Smaller: Effects of Nanomaterials on Microbial Biology, Pathology, and Ecology. *ACS nano*. 2018; **12**(7): 6351-9.

14. Fan, J-X, Li, Z-H, Liu, X-H*, et al.* Bacteria-Mediated Tumor Therapy Utilizing Photothermally-Controlled TNF-α Expression via Oral Administration. *Nano letters*. 2018; **18**(4): 2373-80.

15. McKelvie, ND, Khan, SA, Karavolos, MH*, et al.* Genetic detoxification of an aroA Salmonella enterica serovar Typhimurium vaccine strain does not compromise protection against virulent Salmonella and enhances the immune responses towards a protective malarial antigen. *FEMS Immunol Med Microbiol*. 2008; **52**(2): 237-46.

16. Chen, W, Wang, Y, Qin, M*, et al.* Bacteria-Driven Hypoxia Targeting for Combined Biotherapy and Photothermal Therapy. *ACS nano*. 2018; **12**(6): 5995-6005.

17. Wang, S-B, Liu, X-H, Li, B*, et al.* Bacteria-Assisted Selective Photothermal Therapy for Precise Tumor Inhibition. *Adv Funct Mater*. 2019; **29**(35): 1904093.

18. Luo, C-H, Huang, C-T, Su, C-H*, et al.* Bacteria-Mediated Hypoxia-Specific Delivery of Nanoparticles for Tumors Imaging and Therapy. *Nano letters*. 2016; **16**(6): 3493-9.

19. Liu, L, He, H, Luo, Z*, et al.* In Situ Photocatalyzed Oxygen Generation with Photosynthetic Bacteria to Enable Robust Immunogenic Photodynamic Therapy in Triple-Negative Breast Cancer. *Adv Funct Mater*. 2020; **30**(10): 1910176.

20. Cao, Z, Wang, X, Pang, Y*, et al.* Biointerfacial self-assembly generates lipid membrane coated bacteria for enhanced oral delivery and treatment. *Nat Commun*. 2019; **10**(1): 5783.

21. Wang, X, Cao, Z, Zhang, M*, et al.* Bioinspired oral delivery of gut microbiota by self-coating with biofilms. *Sci Adv*. 2020; **6**(26): eabb1952.

22. Feng, P, Cao, Z, Wang, X*, et al.* On-Demand Bacterial Reactivation by Restraining within a Triggerable Nanocoating. *Adv mater*. 2020; **32**(34): e2002406.

23. Pan, C, Li, J, Hou, W*, et al.* Polymerization-Mediated Multifunctionalization of Living Cells for Enhanced Cell-Based Therapy. *Adv Mater*. 2021; **33**(13): 2007379.

24. Lin, S, Mukherjee, S, Li, J*, et al.* Mucosal immunity-mediated modulation of the gut microbiome by oral delivery of probiotics into Peyer's patches. *Sci Adv*. 2021; **7**(20).

25. Cao, Z, Cheng, S, Wang, X*, et al.* Camouflaging bacteria by wrapping with cell membranes. *Nat Commun*. 2019; **10**(1): 3452.

26. Li, L, Jiang, Y, Cui, C*, et al.* Modulating Aptamer Specificity with pH-Responsive DNA Bonds. *J Am Chem Soc*. 2018; **140**(41): 13335-9.

27. Wu, Y, Zhang, L, Cui, C*, et al.* Enhanced Targeted Gene Transduction: AAV2 Vectors Conjugated to Multiple Aptamers via Reducible Disulfide Linkages. *J Am Chem Soc*. 2018; **140**(1): 2-5.

28. Ouyang, C, Zhang, S, Xue, C*, et al.* Precision-Guided Missile-Like DNA Nanostructure Containing Warhead and Guidance Control for Aptamer-Based Targeted Drug Delivery into Cancer Cells in Vitro and in Vivo. *J Am Chem Soc*. 2020; **142**(3): 1265-77.

29. Zhou, J, Rossi, J. Aptamers as targeted therapeutics: current potential and challenges. *Nat Rev Drug Discov*. 2017; **16**(3): 181-202.

30. Liang, H, Zhang, XB, Lv, Y*, et al.* Functional DNA-containing nanomaterials: cellular applications in biosensing, imaging, and targeted therapy. *Acc Chem Res*. 2014; **47**(6): 1891-901.

31. Sun, H, Zhu, X, Lu, PY*, et al.* Oligonucleotide Aptamers: New Tools for Targeted Cancer Therapy. *Mol Ther- Nucl Acids*. 2014; **3**: e182.

32. Yang, Q, Deng, Z, Wang, D*, et al.* Conjugating Aptamer and Mitomycin C with Reductant-Responsive Linker Leading to Synergistically Enhanced Anticancer Effect. *J Am Chem Soc*. 2020; **142**(5): 2532-40.

33. Xuan, W, Xia, Y, Li, T*, et al.* Molecular Self-Assembly of Bioorthogonal Aptamer-Prodrug Conjugate Micelles for Hydrogen Peroxide and pH-Independent Cancer Chemodynamic Therapy. *J Am Chem Soc*. 2020; **142**(2): 937-44.

34. He, J, Peng, T, Peng, Y, *et al.* Molecularly Engineering Triptolide with Aptamers for High Specificity and Cytotoxicity for Triple-Negative Breast Cancer. *J Am Chem Soc*. 2020; **142**(6): 2699-703.

35. Romano, S, Fonseca, N, Simões, S, *et al.* Nucleolin-based targeting strategies for cancer therapy: from targeted drug delivery to cytotoxic ligands. *Drug Discov Today*. 2019; **24**(10): 1985-2001.

36. Ou, B, Yang, Y, Tham, WL, *et al.* Genetic engineering of probiotic Escherichia coli Nissle 1917 for clinical application. *Appl Microbiol Biotechnol*. 2016; **100**(20): 8693-9.

37. Fan, JX, Peng, MY, Wang, H, *et al.* Engineered Bacterial Bioreactor for Tumor Therapy via Fenton-Like Reaction with Localized H2 O2 Generation. *Adv mater*. 2019; **31**(16): e1808278.

38. Acquah, C, Danquah, MK, Yon, JLS, *et al.* A review on immobilised aptamers for high throughput biomolecular detection and screening. *Anal Chim Acta.* 2015; **888**: 10-8.

39. Hartman, DA. Determination of the Stability of Drugs in Plasma. *Curr Protoc Pharmacol*. 2002; **19**(1): 7.6.1-7.6.8.

40. Yu, J, Yang, L, Liang, X, *et al.* Aptamer and PNIPAAm co-conjugated nanoparticles regulate activity of enzyme with different temperature. *Talanta*. 2016; **159**: 47-54.

41. Liu, X, Yan, H, Liu, Y, *et al.* Targeted cell-cell interactions by DNA nanoscaffold-templated multivalent bispecific aptamers. *Small*. 2011; **7**(12): 1673-82.

42. Tang, Y, Hu, H, Zhang, MG*, et al.* An aptamer-targeting photoresponsive drug delivery system using "off–on" graphene oxide wrapped mesoporous silica nanoparticles. *Nanoscale*. 2015; **7**(14): 6304-10.

43. Liu, H, Sun, N, Ding, P*, et al.* Fabrication of aptamer modified TiO2 nanofibers for specific capture of circulating tumor cells. *Coll Surf B*. 2020; **191**: 110985.

44. Agrawal, N, Bettegowda, C, Cheong, I*, et al.* Bacteriolytic therapy can generate a potent immune response against experimental tumors. *Proc Natl Acad Sci. USA*. 2004; **101**(42): 15172-7.

45. Yoo, J-W, Irvine, DJ, Discher, DE*, et al.* Bio-inspired, bioengineered and biomimetic drug delivery carriers. *Nat Rev Drug Discov*. 2011; **10**(7): 521-35.

46. Gopalakrishnan, V, Spencer, CN, Nezi, L*, et al.* Gut microbiome modulates response to anti-PD-1 immunotherapy in melanoma patients. *Science*. 2018; **359**(6371): 97-103.

47. Imaizumi, K, Suzuki, T, Kojima, M*, et al.* Ki67 expression and localization of T cells after neoadjuvant therapies as reliable predictive markers in rectal cancer. *Cancer sci*. 2020; **111**(1): 23-35.

48. Chen, W, Guo, Z, Zhu, Y*, et al.* Combination of Bacterial-Photothermal Therapy with an Anti-PD-1 Peptide Depot for Enhanced Immunity against Advanced Cancer. *Adv Funct Mater*. 2020; **30**(1): 1906623.

49. Ding, Z, Wang, D, Shi, W*, et al.* In vivo Targeting of Liver Cancer with Tissue- and Nuclei-Specific Mesoporous Silica Nanoparticle-Based Nanocarriers in mice. *Int J Nanomedicine*. 2020; **15**: 8383-400.

50. Geng, Z, Wang, L, Liu, K, *et al.* Enhancing anti-PD-1 immunotherapy by nanomicelles self-assembled from aptamer-multivalent-drug conjugates. *Angew Chem Int Ed*. https://doi.org/10.1002/anie.202102631.

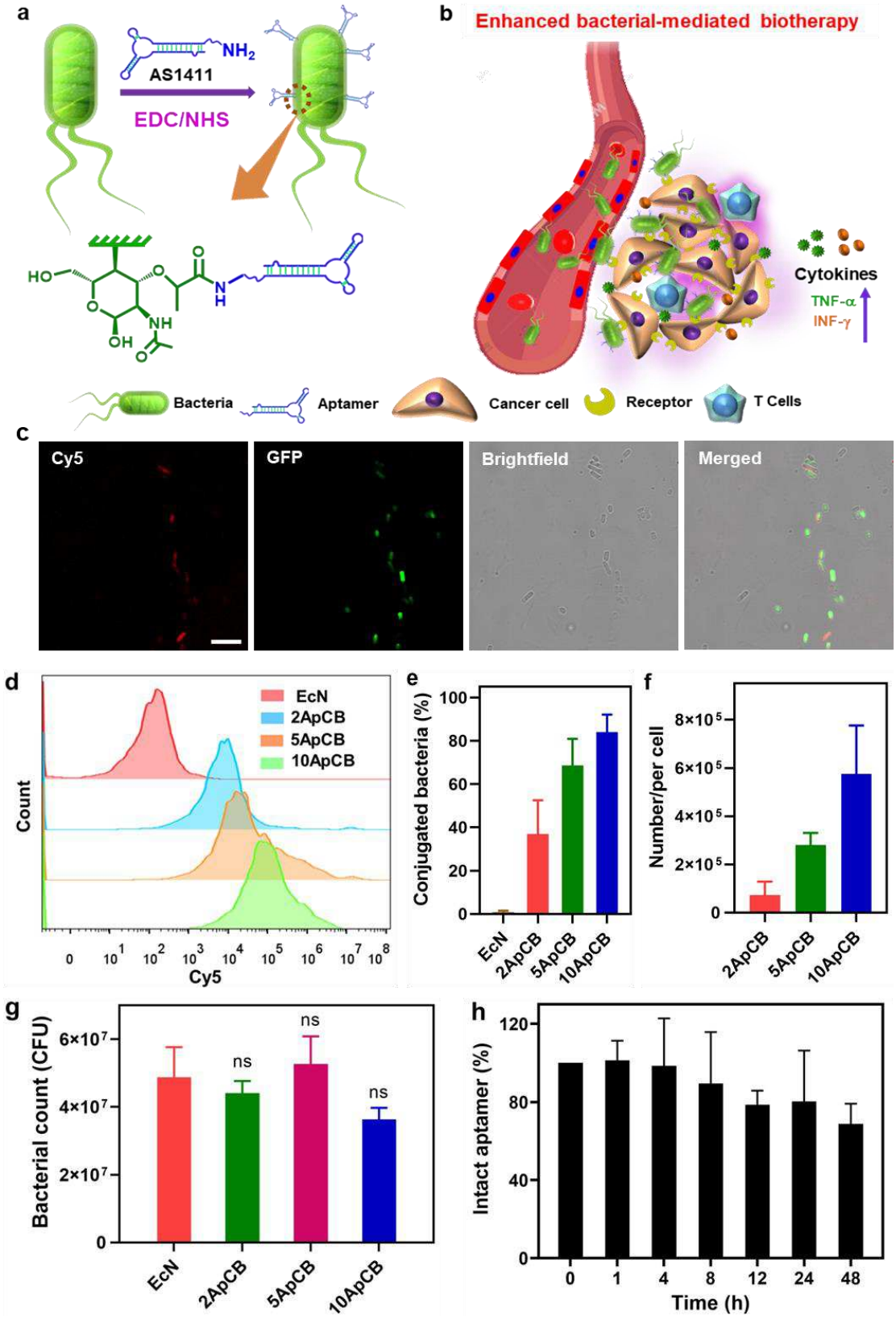

Figure 1. Design, preparation and characterization of ApCB. (a) Preparation of ApCB through amide condensation. (b) Aptamer-assisted tumor localization of bacteria for enhanced biotherapy. (c) Typical LSCM images of aptamer-conjugated bacteria. The red and green channels indicate aptamer conjugated with Cy5 and EcN producing

GFP, respectively. Scale bar: 10 μm. (d) Flow cytometric analysis of EcN and EcN conjugated with Cy5-labelled AS1411. (e) Percentages of conjugated EcN under different feed ratios. (f) Average binding number of aptamers on each bacterial quantified by calculating the difference of fluorescent intensity of the aptamer solution after reaction. (g) Bacterial viabilities of EcN, 2ApCB, 5ApCB, and 10ApCB by LB agar plate counting. Plates were incubated at 37 °C for 24 hours prior to enumeration (n = 3). ns: no significance. (h) Degradation kinetics of the conjugated AS1411 in 90% phosphate-buffered serum solution at 37 °C. ns: no significance.

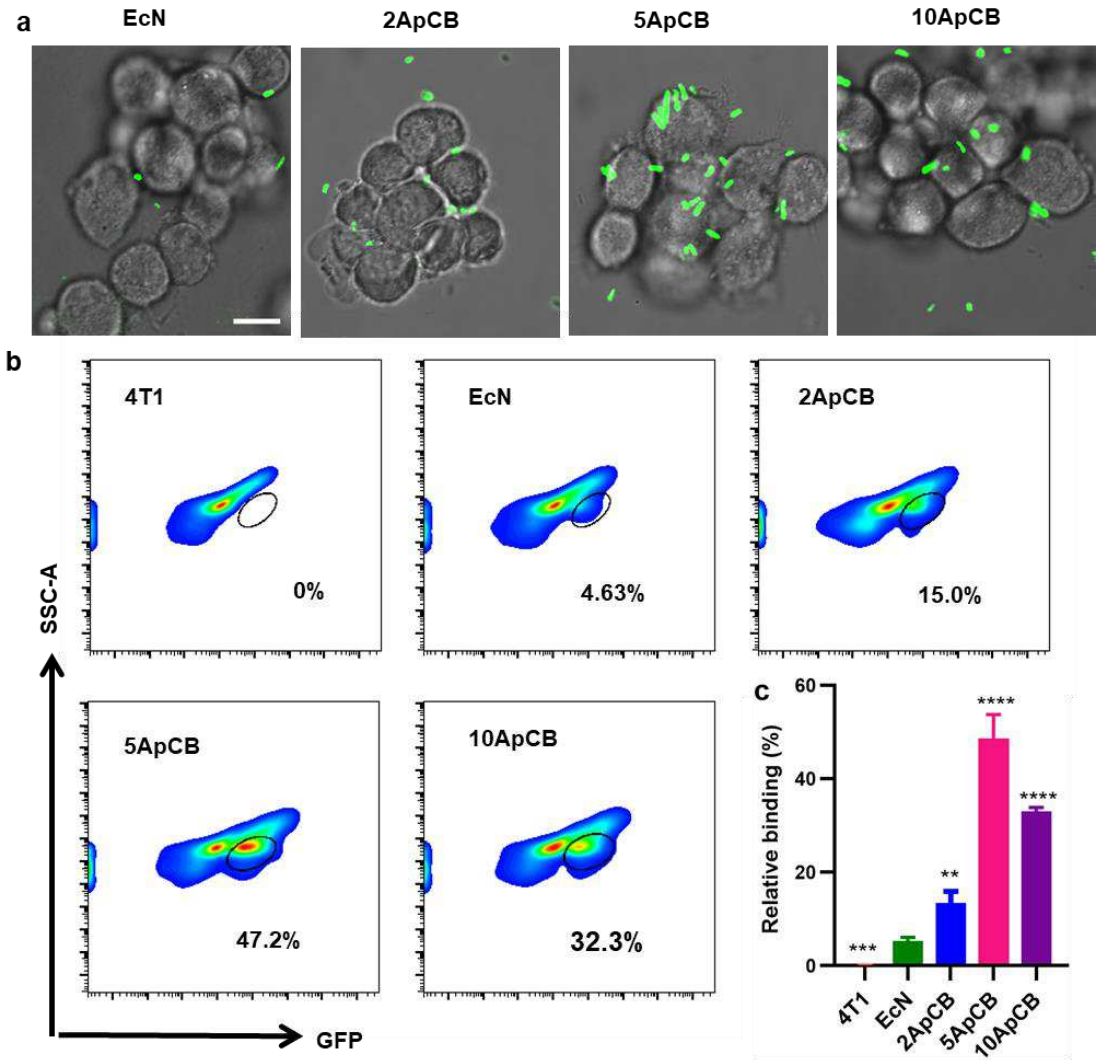

Figure 2. Binding of ApCB with 4T1 cells. (a) Representative LSCM images of 4T1 cells after incubation with EcN, 2ApCB, 5ApCB, and 10ApCB at 37 °C for 2 hours, respectively. Cells were rinsed with PBS before observation. The green channel means EcN producing GFP. Scale bar: 10 μm. (b) Flow cytometric analysis of 4T1 cells after co-incubation with different conjugated EcN at 37 °C for 2 hours. (c) Percentages of 4T1 cells binding with ApCB after co-incubation at 37 °C for 2 hours. Error bars represent the standard deviation (n = 3). Significance was assessed using Student's t-test, giving p-values, $^{**}p < 0.01$, $^{***}p < 0.001$, $^{****}p < 0.0001$.

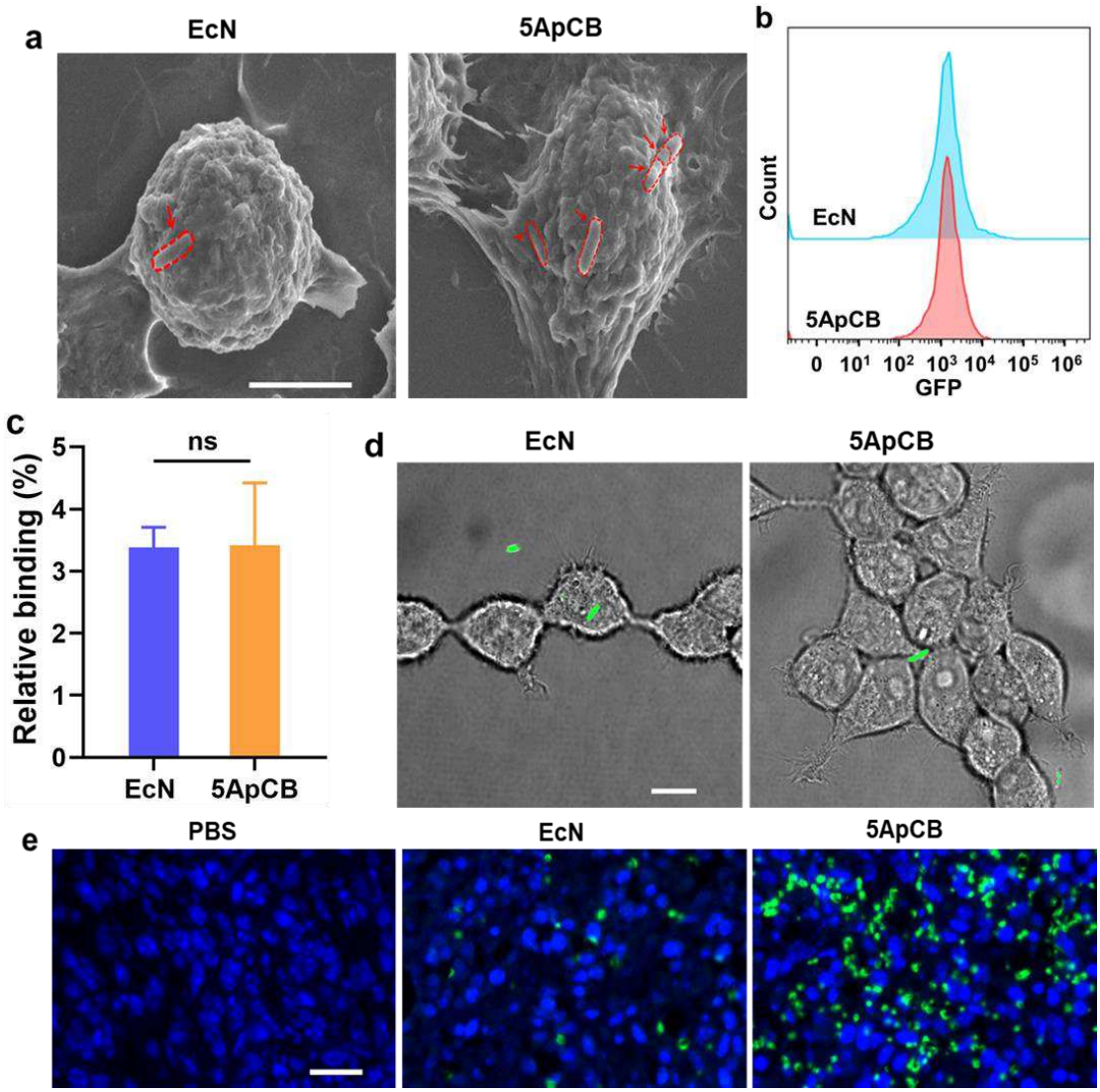

Figure 3. Specific binding of ApCB with cancer cells. (a) Representative SEM images of 4T1 cells after incubation with EcN and 5ApCB at 37 °C for 2 hours, respectively. Bacteria were circled by red dotted line. Scale bar: 5 μm. (b) Flow cytometric analysis of 293T cells after co-incubation with EcN and 5ApCB at 37 °C for 2 hours, respectively. (c) Percentages of 293T cells binding with EcN and 5ApCB after co-incubation at 37 °C for 2 hours, respectively. Error bars represent the standard deviation (n = 3). Significance was assessed using Student's t-test. ns: no significance. (d) Typical LSCM images of 293T cells after incubation with EcN and 5ApCB at 37 °C for 2 hours, respectively. Cells were rinsed with PBS before observation. Green channel means EcN producing GFP. Scale bar: 10 μm. (e) Confocal images of tumor tissues sectioned at 12 hours after intravenous injection of 1×10^7 CFU bacteria. Green and blue indicate EcN stained with Cyanine3-labelled anti-*Escherichia coli* and nuclei stained with DAPI. Scale bar: 20 μm.

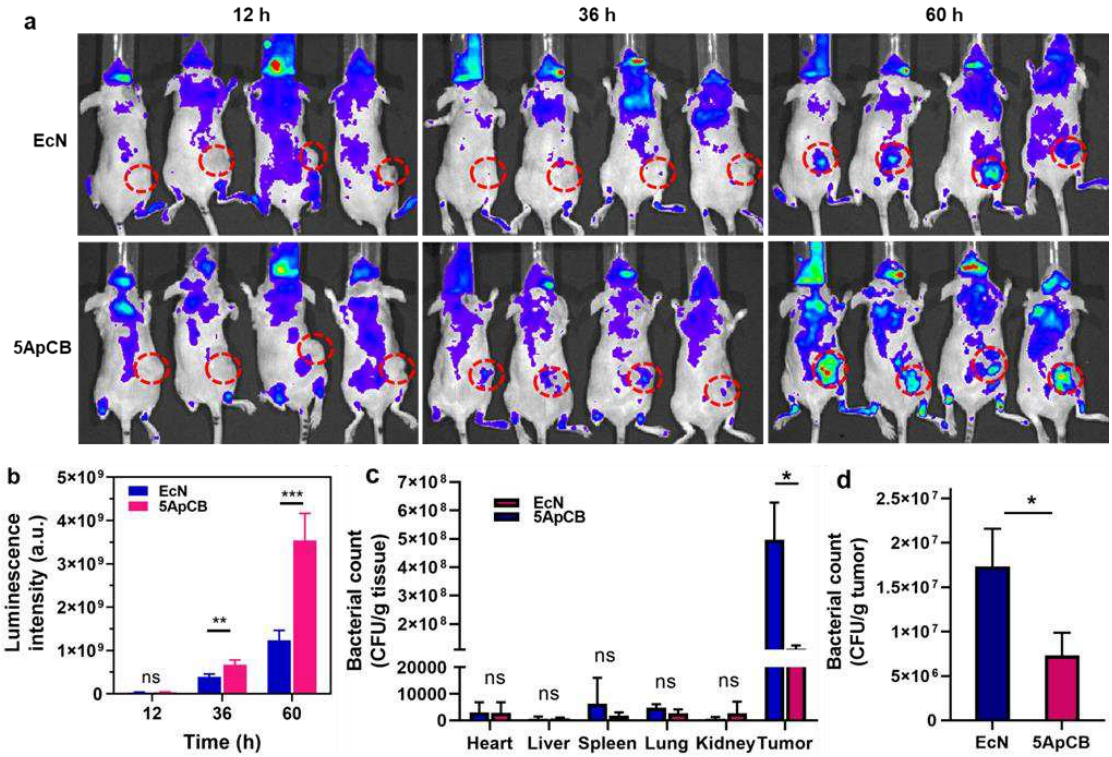

Figure 4. Biodistribution of ApCB in tumor-bearing mice. (a) IVIS imaging of 4T1 tumor-bearing mice at 12, 36, and 60 hours after injection with EcN and 5ApCB (1×10^7 CFU, expressing LuxCDABE) through the tail vein. (b) Average intensity of luminescence signals from the tumor site at 12, 36, and 60 hours after injection. (c) Biodistribution of bacteria in the major organs and tumor tissue of mice at 60 hours after injection with 1×10^7 CFU of EcN or 5ApCB through the tail vein. (d) Numbers of EcN colonized within the tumor at 12 hours after tail vein injection of EcN or 5ApCB. Error bars represent the standard deviation ($n = 4$). Significance was assessed using Student's *t*-test, giving *p*-values, $*p < 0.05$, $**p < 0.01$, $***p < 0.001$. ns: no significance.

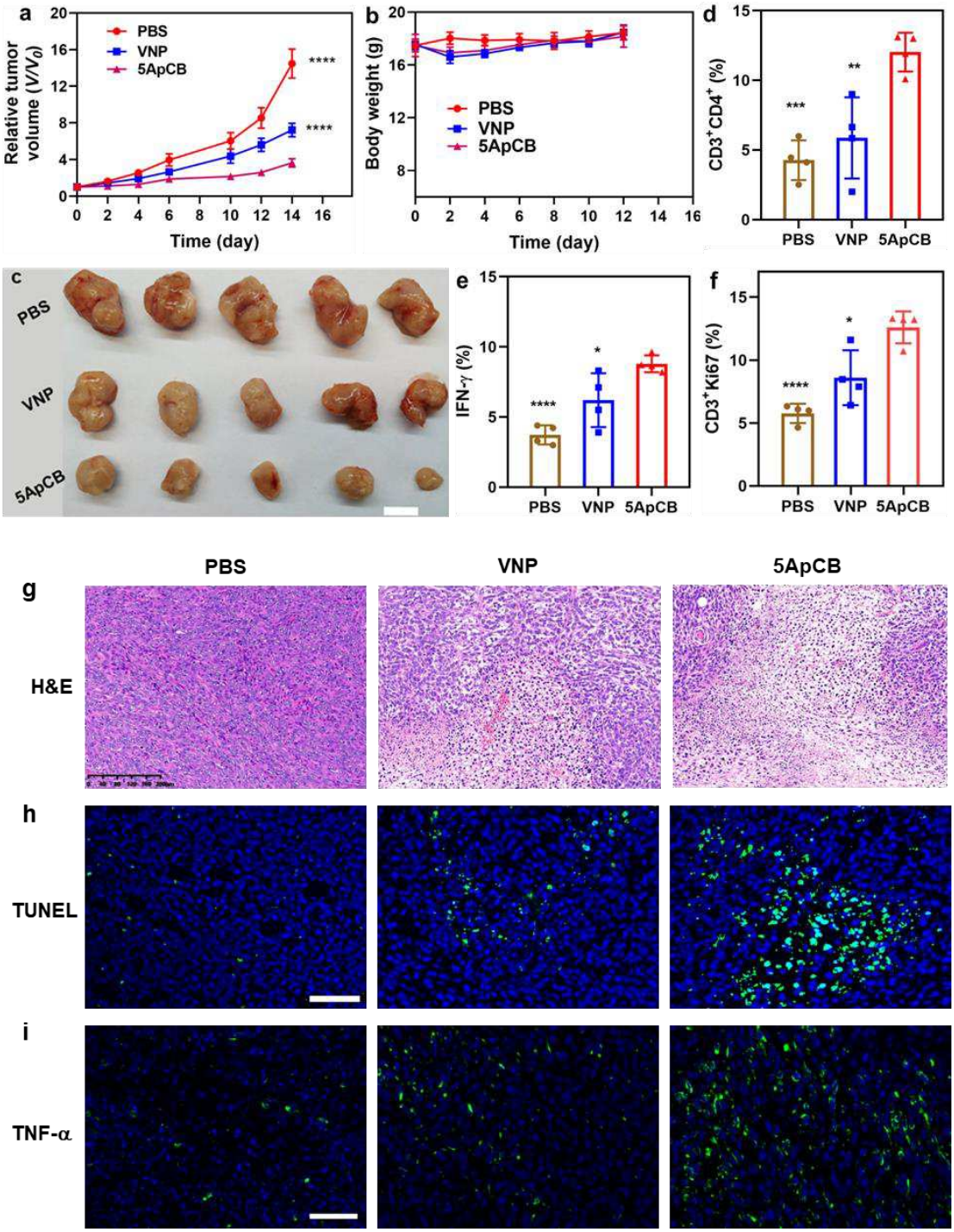

Figure 5. In vivo therapeutic efficacy of ApCB. (a) Relative tumor growth after different treatments (n = 5). (b) Representative photographs of the tumor tissues harvested from mice at the end of the treatment. Scale bar: 1 cm. (c) Variation of bodyweight during each treatment (n = 5). Percentage of (d) Ki67 (gated on $CD3^+$ cells) inside the tumors after treatment (n = 4). (e) Flow cytometric analysis of the population of $CD4^+$ T cells (gated on $CD3^+$ cells) within the tumors after treatment (n = 4). Percentage of (f) IFN-γ (gated on $CD3^+$ cells) inside the tumors after treatment (n = 4). Images of tumor tissues stained with (g) TNF-α and (h) TUNEL. Scale bar: 50 μm. (i) Typical H&E staining images of the sectioned tumors after different

treatments. Scale bar: 200 μm. Significance was assessed using Student's *t*-test, giving *p*-values, *$p < 0.05$, **$p < 0.01$, ***$p < 0.001$, ****$p < 0.0001$.

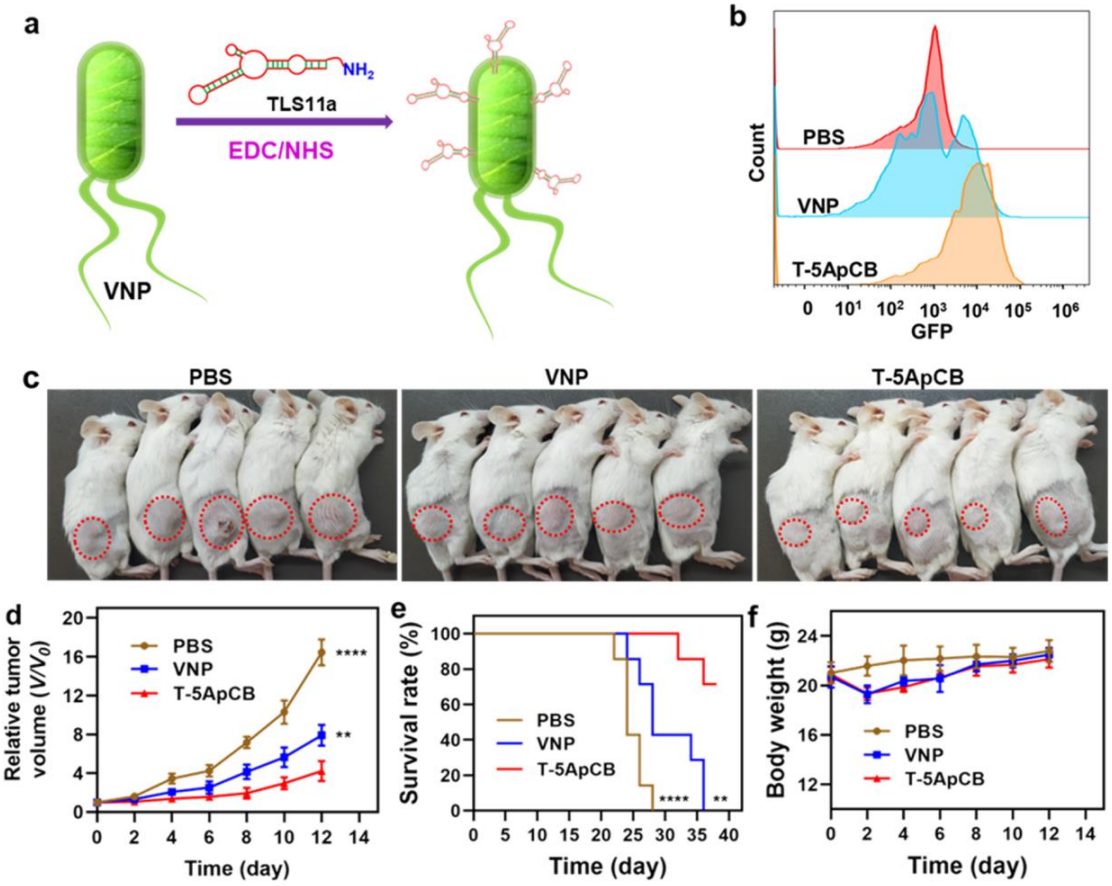

Figure 6. Implementation of ApCB with aptamer TLS11a in a H22 tumor-bearing model. (a) Preparation of ApCB by conjugating VNP with TLS11a via amide condensation. (b) Flow cytometric analysis of H22 cells after co-incubation with PBS, VNP, and T-5ApCB at 37 °C for 1 hour. (c) Digital photos of mice at day 12 after treatment. Tumors were marked in red circles. H22 tumor–bearing mice (inoculated with 1×10^6 carcinoma cells) were randomly divided into three groups and intravenously injected with PBS and 5×10^5 CFU of VNP or T-5ApCB upon tumor size reaching at ~100 mm^3 (defined as day 0). (d) Relative tumor growth after different treatments. (e) Survival curves of H22 tumor-bearing mice after different treatments. (f) Variation of body weight during treatment. Error bars represent the standard deviation (n = 7). Significance was assessed using one-way ANOVA with Tukey post hoc test, giving p values, ** $p < 0.01$, **** $p < 0.0001$.

Supplementary Files

This is a list of supplementary files associated with this preprint. Click to download.

- SupplementaryInformation.pdf